Nickel Nanoparticles Decorated Nitrogen-Doped Carbon Nanotubes (Ni/N-CNT); A Robust Catalyst for the Efficient and Selective CO 2

Nickel Nanoparticles Decorated Nitrogen-Doped Carbon Nanotubes (Ni/N-CNT); a Robust Catalyst for the Efficient and Selective CO_2 Methanation

Wei Wang, [ξ,§] Cuong Duong-Viet,*[, ξ, ‡, §] Housseinou Ba,[ξ] Walid Baaziz,[φ] Giulia Tuci,[δ, ε] Stefano Caporali,[ε] Lam Nguyen-Dinh,[γ] Ovidiu Ersen,[φ] Giuliano Giambastiani,*[, ξ, δ] and Cuong Pham-Huu*[,ξ]

[ξ] *Institut de Chimie et Procédés pour l'Energie, l'Environnement et la Santé* (ICPEES), ECPM, UMR 7515 du CNRS-Université de Strasbourg, 25 rue Becquerel, 67087 Strasbourg Cedex 02, France.

[‡] *Ha-Noi Univ*. of Mining and Geology, 18 Pho Vien, Duc Thang, Bac Tu Liem, Ha-Noi, Vietnam.

[φ] *Institut de Physique et Chimie des Matériaux de Strasbourg* (IPCMS), UMR 7504 du CNRS-Université de Strasbourg, 23 rue du Loess, 67037 Strasbourg Cedex 03, France

[δ] *Institute of Chemistry of OrganoMetallic Compounds*, ICCOM-CNR and Consorzio INSTM, Via Madonna del Piano, 10 – 50019, Sesto F.no, Florence, Italy

[ε] *Department of Chemistry "Ugo Schiff"*, University of Florence, 50019, Sesto F.no, Florence, Italy

[γ] *The University of Da-Nang*, University of Science and Technology, 54, Nguyen Luong Bang, Da-Nang, Vietnam

[§] *These authors contributed equally to the work*

ABSTRACT. Carbon dioxide (CO_2) hydrogenation to methane (CH_4) is a way of great significance from an energy-saving viewpoint that consists in the direct conversion of a natural and abundant waste into a fuel of added value. Its practical exploitation can significantly impact on the control of anthropogenic CO_2 emissions into the Earth's atmosphere and their dramatic effects in terms of global warming, environmental impact and climate changes. Moreover, the conjugation of CO_2 with H_2 from renewable resources (RE) is at the forefront of modern chemical technologies for RE storage. Indeed, it can be used to provide synthetic CH_4 as an alternative source to natural gas to be potentially injected in the existing gas grid.

This contribution describes the synthesis of a robust catalyst for the efficient and selective CO_2 methanation, based on Nickel nanoparticles (Ni-NPs) grown on N-doped carbon nanotubes

(Ni/N-CNT). The high thermal conductivity of N-CNT ensures a good dispersion of the reaction heat throughout the catalyst bed while N-doping lists a number of key and distinctive catalyst features: a) it provides preferential binding sites for the Ni-NPs stabilization, b) it contributes to generate CO_2 concentration gradients in proximity of the catalyst active phase and c) it largely prevents the formation of coke deposits (catalyst passivation) on stream. The as prepared catalyst shows superior methanation activity and selectivity compared to those claimed for the most representative Ni-based composites reported so far in the literature. Importantly, the Ni/N-CNT displays its better performance in CO_2 methanation under severe reaction conditions, *i.e.* high temperatures and GHSV (up to 120,000 mL g^{-1} h^{-1}) where it unveils an excellent stability as a function of time-on-stream.

KEYWORDS: CO_2 methanation; Chemical energy storage; N-doped carbon nanotube; Nickel nanoparticles; Basic supports

1. INTRODUCTION

The intensification of all main anthropic activities together with the growing need of worldwide citizens' connections and goods transportations are facing with a steadily increasing energy demand. At the same time, the request of reducing CO_2 emissions, prevalently raising from an uncontrolled use of fossil fuels, is becoming a more and more urgent priority of our modern society. Indeed, CO_2 emissions contribute to the so-called "greenhouse effect" with severe implications in terms of global warming, heavy environmental impact and related weather changes.[1] To cope with this dramatic scenario, new European directives have been established with the aim of replacing fossil fuels by renewable energy sources (RE). By this way, it is expected that global greenhouse gas emissions will be reduced by 80-95 % before

2050[2] and REs will play a key role in the electric power generation of more developed countries at the dawn of 2030.

To date, three main approaches are systematically pursued to reduce CO_2 emissions: 1) limit the utilization of fossil resources; 2) develop new systems for the CO_2 capture and sequestration (CCS); 3) valorize CO_2 by converting and employing it for the production of chemicals and energy vectors of added value (Carbon Capture and Valorization - CCV).[3] CCV, in particular, is highly preferable compared to CCS in the perspective of ensuring a long-term and sustainable development of our society. It moves from a radically new view-point where CO_2 is no longer regarded as a simple waste but rather as a renewable resource to be harvested and recycled into carbon-containing products and feedstock of added value. To accomplish this challenging task, well defined catalytic strategies and energy input are required. The conjugation of CO_2 conversion with REs can foster the process in terms of both sustainability and environmental friendliness. On this regard, CO_2 hydrogenation[4-7] using H_2 from RE sources[1, 8] is a highly promising approach that meets with several key challenges of a modern society. Indeed, it represents a sustainable method to the production of chemicals and fuels[9-16] from renewable sources. Moreover, it copes with the main environmental and climate urgencies directly linked to steadily state increase of CO_2 concentration in the atmosphere. Catalytic hydrogenation of CO_2 with RE H_2 is nowadays at the forefront of many chemical technologies devoted to the production of low molecular weight olefins,[17] hydrocarbons,[18] formic acid,[19] and alcohols.[20-22] Most importantly, it can cope with the steady depletion of fossil resources by providing a synthetic way to natural gas (SNG) as fuel. The ‘‘power to gas’’ (PtG) concept deals with the reaction of CO_2 with RE H_2 produced by water electrolysis[23-25] promoted by wind or solar power, to give CH_4 (CO_2 methanation) as an alternative synthetic source to natural gas. PtG contributes to store the surplus power from RE sources into SNG thus linking the existing power networks to natural gas grids.[3] The synthetic methane can be either injected into the

existing natural gas pipelines, or directly employed as raw material for the production of other commodities.[25-27] Nowadays, two main methanation processes are operated through different pilot and industrial plants, namely the catalytic and biological methanation. As for the former, several metal-active phases, typically based on Ni, Ru, Pd nanoparticles (NPs) on various oxide supports (i.e. TiO_2, SiO_2, Al_2O_3, CeO_2, MgO and ZrO_2)[28-32] have been successfully employed in the transformation, with Ni-based catalysts being among the most investigated systems.

CO_2 methanation is an exothermic process (ΔH = -165 kJ mol^{-1}) and high temperatures can deeply affect CO_2 conversion and selectivity or even induce permanent catalyst deactivation through metal NPs sintering, leaching or active sites encapsulation by coke deposits. For this reason, high gas hourly space velocity (GHSV), typically over 10,000 h^{-1}, are required for the process to occur efficiently. Indeed, high GHSV values ensure a more efficient gas-heat exchange and limit the generation of gradients of temperature throughout the catalyst bed. The excess of local heat produced by the reaction has to be properly managed in order to limit as much as possible the generation of undesired "hot spots" responsible in turn for the reduced catalyst life-time and process selectivity.

To this aim various type of reactors, *i.e.* adiabatic fixed-bed reactors, fluidized-bed reactors or structured three-phase reactors, have been applied to the process.[33-37] Recent outcomes have pointed out how the use of thermal conductive supports, preferably featured by high specific surface area and open cells porosity, hold beneficial effects on the process efficiency by limiting the generation of local hot spots inside the catalyst bed.[38-42] In addition, supports containing preferential anchorage sites to strongly tether metal NPs bring additional advantages to the heterogeneous system such as a better dispersion of the metal active phase (in the catalyst preparation step) or a minor occurrence of leaching and sintering phenomena during the hydrogenation process.

This is the case of light-doped nanocarbon supports (*e.g*. nanotubes, N-CNTs[43] or nanofibers, N-CNFs[40]) where hetero-elements (*i.e*. N-sites) at the outer material surface contribute to control the NPs growth and their distribution while ensuring improved stability to the composite in catalysis. In addition, nanocarriers featured by basic surface properties are highly desirable in the case of processes involving CO_2 conversion and valorization (CCV). Indeed, basicity is supposed to foster the generation of local gradients of CO_2 concentrations neighboring the catalyst metal active sites. On this ground, Roldan *et al*.[40] have recently demonstrated the positive influence played by basic N-doped carbon nanofibers (N-CNFs) as support for Ru NPs in CO_2 methanation. Hao *et al*.[44] have also stressed the role of basicity for specific N-dopants engaged in the interaction with CO_2 for its activation/conversion. Similarly, Ussa Aldana and co-workers[45] have shown the importance of weak basic sites available at the support of their Ni-ceria-zirconia methanation catalyst on the improvement of its ultimate performance. It is also known from the literature that CO_2 interaction with selected basic supports can change the pristine geometry of carbon dioxide, bending the molecule and lowering the kinetic barrier associated to its reduction process.[46-47]

Supports basicity is finally known to have an influence on CO_2 methanation selectivity. This is the case of MgO-promoted SiO_2 supports decorated with Pd NPs. Park and MacFarland[48] have observed a dramatic change in the process selectivity upon MgO doping of silica particles. Indeed, Pd/SiO_2 catalyst provides almost exclusively CO as reduction product whereas CH_4 is predominant when the MgO-promoted catalyst is at work.

In this contribution we describe the synthesis of Ni-NPs decorated N-doped carbon nanotubes (Ni/N-CNT) as a robust catalyst for the efficient and selective CO_2 methanation. The high thermal conductivity of N-CNT support ensures a good dispersion of the reaction heat throughout the catalyst bed. N-doping in the nanocarrier holds a dual key role: 1) it provides preferential binding sites for the Ni-NPs growth and stabilization and, 2) it concentrates CO_2 in

proximity of the catalytically active phase thus ensuring superior methanation performance than that claimed for the most representative Ni-based composites reported so far.[38, 49-67] Importantly, the Ni/N-CNT catalyst displays its better performance and stability for CO_2 methanation under severe reaction conditions, *i.e*. high temperatures and GHSV up to 120,000 mL g^{-1} h^{-1} where it also demonstrates an excellent stability as a function of time-on-stream.

2. MATERIALS AND METHODS

Nitrogen-doped carbon nanotubes (N-CNTs) have been synthesized by Chemical Vapour Deposition (CVD), using a $C_2H_6/NH_3/H_2$ mixture in a 2/2/1 molar ratio, according to literature procedures previously described by some of us.[68-69] The synthesis was carried out at 750 °C for 2 h and the crude product was finely crushed before undergoing a classical washing/purification procedure. Nickel NPs were deposited on N-CNTs by incipient wetness impregnation,[70] using an aqueous solution of nickel nitrate [$Ni(NO_3)_2.6H_2O$] as to get a theoretical metal loading closed to 10 wt.%. The oven-dried catalyst was calcined in air at 350°C for 2 h as to convert the nickel nitrate into its oxide counterpart. Afterwards, NiO/N-CNT underwent a reduction step at 350°C for 2 h under a dynamic stream of H_2 (100 mL min^{-1}). Nickel loading was fixed by *Inductively Coupled Plasma Atomic Emission spectrophotometry* (ICP-AES) after complete acidic mineralization of NiO/N-CNT sample, using an Optima 2000 Perkin Elmer Inductively Coupled Plasma (ICP) Dual Vision instrument; the effective nickel charge was then fixed to 10.7 wt.%.

$N\text{-}CNT_{calc.}$ were prepared using the identical calcination treatment described above for the Ni-based composite. Similarly, hydrogenation of $N\text{-}CNT_{calc.}$ to give $N\text{-}CNT_{H2}$ was carried out under conditions identical to those applied above for the reduction of NiO/N-CNT composite.

Scanning electron microscopy (SEM) was conducted on a ZEISS GeminiSEM 500 microscope with a resolution of 5 nm. For each measurement, samples were deposited onto a double face graphite tape in order to avoid charging effect during the analysis. *Transmission Electron Microscopy* (TEM) was carried out on a JEOL 2100F microscope working at 200 kV accelerated voltage, equipped with a probe corrector for spherical aberrations, and a point-to-point resolution of 0.2 nm. For these measurements, samples were previously dispersed in ethanol using ultrasounds (for few minutes) till a homogeneous dispersion is obtained and the resulting inks are drop-casted on a copper grid covered with a holey carbon membrane. The *Brunauer-Emmett-Teller* (BET) *specific surface areas* (SSA) were calculated from N_2 physisorption isotherms recorded at 77 K on an ASAP 2020 Micromeritics® instrument. All samples were degassed/activated at T = 250 °C for 8 h prior their characterization. *Thermal gravimetric analysis* (TGA) and *differential thermal gravimetric* (DTG) analysis were run in the 50-800 °C temperature range (heating rate of 10 °C/min) using a TGA Q5000 instrument operating under an air flow (25 mL min^{-1}). Samples weights were roughly maintained around 10 mg each. *Acid-base titration.* In a model experiment, 5 mg of N-$CNT_{(calc\ or\ H2)}$ were suspended in 7 mL of a HCl standard solution (2.8 x 10^{-3} M, standardized with Na_2CO_3 as primary standard), sonicated for 1 h in a water-ice bath and stirred at room temperature for 48 h. Afterwards, the suspension was centrifuged and three aliquots of the supernatant solution were titrated with a standardized solution of NaOH (2 x 10^{-3} M). The amount of surface basic sites was calculated as average value over three independent titration runs.

2.1 CO_2 methanation activity tests. The CO_2 methanation reaction (Eq. 1) was carried out under atmospheric pressure in a fixed-bed tubular reactor (∅ 12 mm, length of 600 mm) charged with 200 mg of the NiO/N-CNT catalyst, packed between quartz wool plugs. A thermocouple was placed inside the catalyst bed as to follow the reaction temperature throughout the whole methanation process. The reactor was finally housed inside an electric

furnace controlled by a second thermocouple for the monitoring of the temperature ramp. Prior of each experiment, the calcinated NiO/N-CNT catalyst was reduced at 350 °C for 2 h under a stream of H_2 (100 mL min^{-1}) and the target temperature was reached at a rate of 10 °C/min. Afterwards, the catalyst was slowly cooled to ambient temperature under a pure He flow before being exposed to the reactive feed (H_2 and CO_2) and heated again to the target reaction temperature. The feed molar composition was finely tuned by a series of calibrated Mass Flow Controllers (Brookhorst®). Gases at the reactor outlet pass through a trap where formed water is condensed before reaching a gas chromatograph (GC, Varian 3800) equipped with TCD and FID detectors and CP Carbobond and DB-1 packed-columns for analysis.

$$CO_2 + 4\,H_2 \rightarrow CH_4 + 2\,H_2O \qquad \Delta H = -165\ kJ/mol \qquad \text{(Eq. 1)}$$

CO_2 conversion (X_{CO2}) and CH_4 selectivity (S_{CH4}) were calculated according to the following equations (Eq. 2 and 3):

$$CO_2 \text{ conversion: } X_{CO_2}(\%) = \frac{F_{CO_2(in)} - F_{CO_2(out)}}{F_{CO_2(in)}} x100 \qquad \text{(Eq. 2)}$$

$$CH_4 \text{ selectivity: } S_{CH_4}(\%) = \frac{F_{CH_4(out)}}{F_{CH_4(out)} + F_{CO(out)}} x100 \qquad \text{(Eq. 3)}$$

Where $F_{CO_2(in)}$ (mL/min) is the volume of CO_2 admitted to the reactor and $F_{CO_2(out)}$ (mL/min) is the volume of CO_2 measured at the reactor outlet. This latter was calculated using the total volume at the reactor outlet and considering the percentage of CO_2 detected by GC analysis. The CH_4 selectivity (S_{CH4}) was calculated by GC analysis considering CO as the unique reaction by-product. During the reaction the large part of the steam formed was condensed at the bottom of the reactor.

3. RESULTS AND DISCUSSION

3.1 Material synthesis and characterization. Figure 1A deals with the SEM micrograph of in-house prepared and purified N-CNT sample (see Materials and Methods section for details). They consist in highly entangled matrices of high aspect-ratio carbon nanotubes. Medium magnification TEM micrograph (Figure 1B) reveals the relatively homogeneous size distribution of N-CNTs diameters (average value of 50 ± 5 nm) along with their typical bamboo-like morphology featured by periodical capping structures alternate to empty compartments all along the tube axis.[71-74] High magnification TEM micrograph (Figure 1C) shows the lack of amorphous carbon layers and prismatic-like graphite sheets all along the tube axis while reveals the existence of highly defective layers. Previous investigations from some of us using EELS-STEM method have shown that N-sites available at the nanomaterial surface are randomly distributed and prevalently located in the correspondence of defective sites.[75]

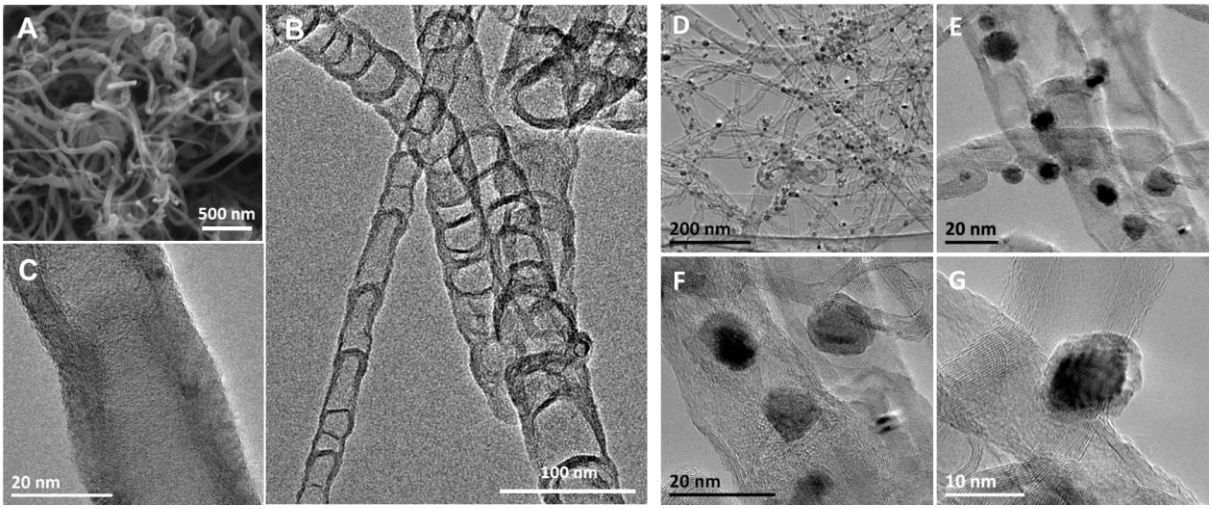

Figure 1. SEM (A) and TEM micrographs (B-G) of the N-CNTs support (A-C) and Ni/N-CNT composite (D-G) at various magnifications. TEM micrographs D-G refer to the Ni/N-CNT after calcination/reduction steps. High-resolution images F-G, demonstrate the presence of a thin layer coating of NiO around Ni-NPs originated just after material exposure to air for few hours.

The specific surface area (SSA) of N-CNTs sample (BET), measured from the N_2 adsorption-desorption branches recorded at the liquid N_2 temperature, is 143 m^2g^{-1} with a total

pore volume of 0.6 $cm^3\ g^{-1}$. Such a value is typical for mesoporous solids and it is in excellent accord with our literature precedents on the topic.[43] Ni-NPs deposition is obtained by incipient wetness impregnation of N-CNTs sample using an aqueous solution of nickel nitrate [$Ni(NO_3)_2{\cdot}6H_2O$] followed by calcination/reduction treatment (see Materials and Methods section for details).[38] The Ni-NPs distribution is analyzed by TEM microscopy and the corresponding images are presented in Figures 1D-G. Low and medium magnification TEM micrographs (Figures 1D-E) reveal the homogeneous and relatively narrow dispersion of Ni-NPs sizes at the N-CNT matrix (*ca*. 10 ± 3 nm, determined from a statistical TEM analysis carried out on more than 200 particles – see also Figure 4C). Such a good control on NPs size and distribution is ascribed to the non-innocent action played by N-dopants available at N-CNTs surface. They control NPs growth and largely prevent agglomeration phenomena during the material thermal treatments.[40, 43] High resolution TEM images of Ni/N-CNT (Figures 1F-G) reveal the presence of a thin coating of NiO around NPs, originated by the material exposure to air just after few hours. The effective amount of deposited Ni (wt.%) has been fixed to 10.7 wt.% by ICP-AES (see Materials and Methods section)

3.2 CO_2 methanation trials with Ni/N-CNT as catalyst: the influence of the reaction temperature. In a typical methanation run, 200 mg of catalyst are packed inside a tubular reactor and pre-treated for 2 h at 350 °C under a stream of pure hydrogen. Afterwards, the temperature system was fixed at the desired target temperature and a H_2/CO_2 mixture (from 4 to 6 v/v ratio) is introduced downward through the catalyst bed at ambient pressure (1 atm) and at a GHSV of 60,000 mL $g^{-1}\ h^{-1}$ (see Materials and Methods section for details). CO_2 conversion (X_{CO2}) and CH_4 selectivity (S_{CH4}) measured at various reaction temperatures (H_2/CO_2 = 4 v/v ratio) are outlined in Figure 2. According to literature precedents, X_{CO2} steadily increases while increasing the reactor temperature in the 200-360 °C range and it rapidly approaches (over 300 °C) conversion values close to those of the thermodynamic equilibrium (Figure 2, dashed

line).[58, 76-77] Methane selectivity (S_{CH4} - not shown in figure for the sake of clarity), constantly lies close to 99% (if not above) throughout the whole temperature range.

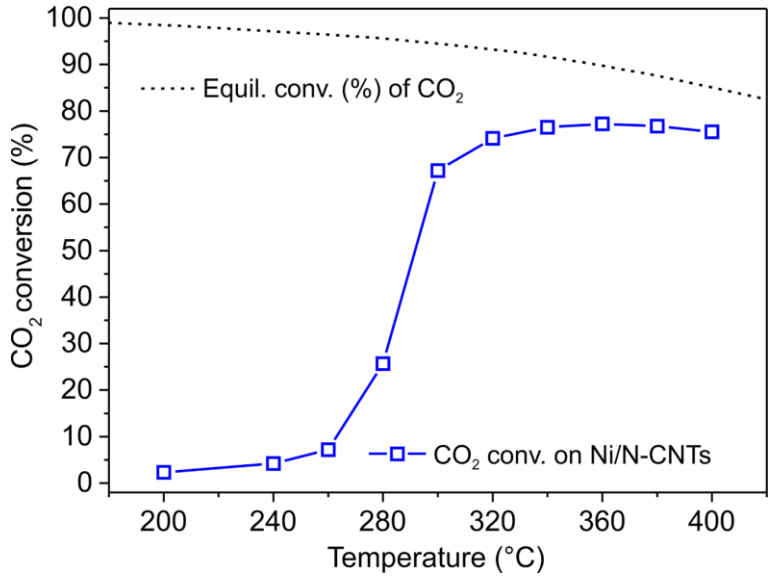

Figure 2. CO_2 methanation with Ni/N-CNT as a function of the reaction temp. (–□–). The catalyst was tested without any thermic diluent. Reaction conditions: catalyst weight = 200 mg, GHSV (STP) = 60,000 mL g^{-1} h^{-1}, CO_2 = 20 mL, H_2 = 80 mL, He = 100 mL, H_2/CO_2 = 4 v/v ratio, atmospheric pressure. Thermodynamic equilibrium conversion (dashed black line "**.....**") has been included for the sake of comparison.

At higher temperatures, (*i.e.* > 360 °C) a slight decrease of X_{CO2} is observed together with a decrease of S_{CH4}, the latter mainly due to the occurrence of side processes *i.e.* steam reforming, water-gas shift or reverse water-gas shift reactions.[78-80] According to the observed trend, the target reaction temperature of 360 °C has been fixed for all methanation runs with Ni/N-CNT. Under these conditions, the catalyst presents a long-term catalytic methanation activity with virtually constant performance even after several hours on stream (*vide infra*). The activation energy for the process with Ni/N-CNT as catalyst (38 kJ mol^{-1}) has been calculated from the Arrhenius plot as the logarithm of CO_2 conversion *vs*. the reciprocal of reaction temperature (Figure S1).

3.3 Influence of GHSV and H_2/CO_2 ratio on the Ni/N-CNT methanation performance and the dual role played by the nanocarrier surface basicity. Besides improving the plant productivity, catalysts operating under high GHSV typically allow a better control on the local

hot spots generation due to a faster heat removal from the catalytic bed (gas-heat exchange). Catalysts featured by low reagents diffusion paths and high intrinsic methanation activity are ideal for operating under conditions where high mass and heat transfer take place. Moreover, to cope with the effective costs related to hydrogen storage and fluctuation of its supply together with variable CO_2 concentrations depending to its source, dynamic operating modes (where both H_2-to-CO_2 v/v ratio and GHSV can change during the process) are highly preferred to run methanation reactions. On the other hand, dynamic conditions can induce the formation of temperature gradients on the catalytic bed as well as high steam concentrations responsible for the occurrence of side processes and decrease of methanation selectivity.

Ni/N-CNT was initially employed for CO_2 methanation at 360 °C under variable H_2-to-CO_2 v/v ratios (from 4 to 6), using two different GHSVs (60,000 and 120,000 mL g^{-1} h^{-1}). Results are summarized in Figure 3. As Figure 3A shows, at the catalyst steady-state conditions, the increase of GHSV from 60,000 to 120,000 translates into a moderate decrease of CO_2 conversion (from 80 to 73 %) together with a slight reduction of S_{CH4} (from 99 to 94 %). Such a trend is in accord with the increased mass transfer and heating in the process and reveals at the same time the excellent catalyst performance when it is requested to operate under more severe conditions (higher GHSV values). Notably, no appreciable deactivation phenomena are observed for the whole process and at the various GHSVs. In a dedicated long-term evaluation trial (Figure 3B), CO_2 methanation is conducted for more than 60 h at 360 °C under a H_2-to-CO_2 ratio of 4 at a GHSV of 60,000 mL g^{-1} h^{-1}. This trial shows the excellent catalyst stability as a function of time-on-stream without any appreciable catalyst alteration throughout the whole process.

When CO_2 methanation is run under higher H_2-to-CO_2 v/v ratio (from 4 to 6, Figure 3C), keeping constant both reaction temperature (360 °C) and GHSV (60,000 mL g^{-1} h^{-1}), CO_2 conversion grows markedly (from 81 to 96 %). This result is in line with a higher density of

dissociated hydrogen at the catalyst surface. On the other hand, S_{CH4} shows an opposite trend and it slightly decreases from 99 to 97 %. Indeed, at a higher CO_2 conversion per unit of time, temperature and steam concentration at the catalyst bed is expected to increase thus making more competitive the occurrence of side processes. At higher GHSV (120 K mL g^{-1} h^{-1}, Figure 3D), the higher the H_2-to-CO_2 v/v ratio the higher the catalyst performance in terms of CO_2 conversion and CH_4 selectivity. Accordingly, X_{CO2} and S_{CH4} grow from 75 to 92 % and from 94 to 98 %, respectively, by increasing the H_2-to-CO_2 v/v ratio from 4 to 6 (Table S1, entries 2 *vs*. 3). Once again, the catalyst displays an extremely high stability as a function of time-on-stream without any apparent deactivation in spite of more severe and fluctuating reaction conditions (H_2-to-CO_2 v/v ratio and GHSVs).

CO_2 methanation performance with Ni/N-CNT as catalyst (X_{CO2}, S_{CH4} and Specific catalyst rate expressed as $mol_{CH_4} \cdot g_{Ni}^{-1} \cdot h^{-1}$) is summarized in Table S1 and compared with the most representative Ni-based catalysts of the *state-of-the-art* operating under similar conditions. These authors are aware about the difficulty of such comparative task because it is made hard by the different conditions used with various catalytic systems (*i.e*. target reaction temperature, H_2-to-CO_2 v/v ratio and GHSV). Nonetheless, from a careful analysis of data outlined in Table S1 it can be inferred that Ni/N-CNT ranks among the most active and selective systems for CO_2 methanation between those operating from medium to high GHSVs with a H_2-to-CO_2 v/v ratio comprised between 3 and 6. In particular, it provides rates close to 5 $mol_{CH_4} \cdot g_{Ni}^{-1} \cdot h^{-1}$ when GHSV is fixed to 120 K mL g^{-1} h^{-1} and H_2-to-CO_2 v/v ratio of 6. This is unambiguously the highest specific rate reported so far for Ni-based catalysts in CO_2 methanation and it largely outperforms the majority of Ni-based systems reported to date in the literature (Table S1). Such a high value is ascribed to several catalyst features, including short reagents diffusion paths due to the nanoscopic dimensions of the catalyst support and the localization of the catalyst active

phase (Ni-NPs) at the outer nanomaterial surface only (virtually no nanoparticles confinement is present into the material pores).

This latter aspect is particularly relevant and distinctive for this class of nanoscopic supports compared to other and more traditional porous carriers. Indeed, the localization of the active phase at the outer surface of the support makes it completely accessible to reactants that is of relevance for processes operated at high GHSVs.

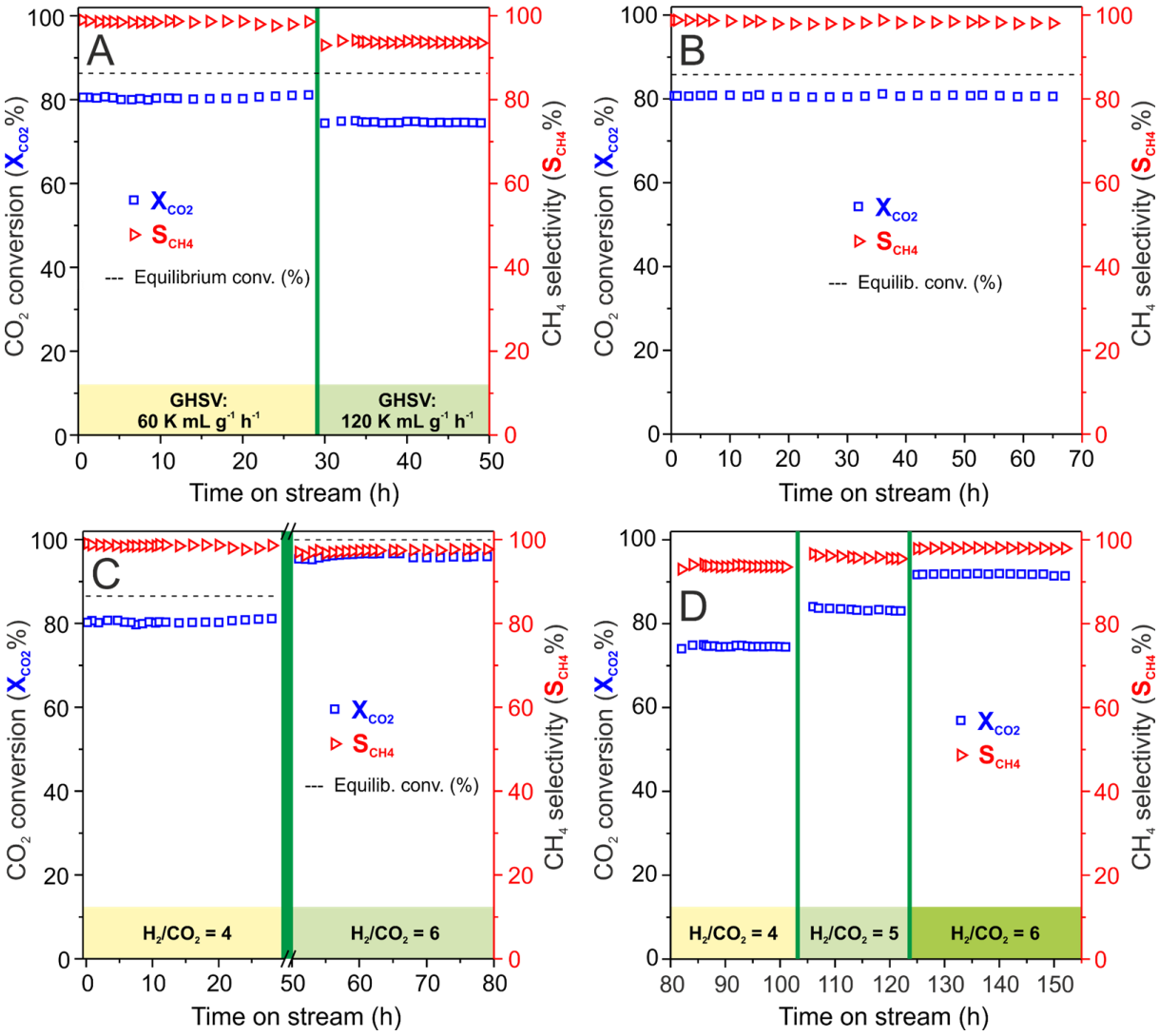

Figure 3. CO_2 methanation runs on Ni/N-CNT catalyst (200 mg) at 360 °C and ambient pressure; catalyst was tested without thermic diluent. Dashed black lines refer to the calculated thermodynamic equilibrium conversion values.[3] A) Influence of GHSV on the process activity and selectivity (from 60 to 120 K mL g^{-1} h^{-1}); B) long-term stability test at a GHSV of 60 K mL g^{-1} h^{-1}; C) Effect of H_2/CO_2 ratio on the process activity and selectivity at a GHSV of 60 K mL g^{-1} h^{-1}; D) Effect of H_2/CO_2 ratio on the process activity and selectivity at a GHSV of 120 K mL g^{-1} h^{-1}.

Finally, the basic character of the NPs carrier is claimed to contribute to the ultimate material performance in methanation catalysis. Indeed, basicity at the nanocarrier surface fosters the generation of local gradients of CO_2 concentration neighboring to metal active sites. It has to be noticed that the calcination treatment used to convert nickel nitrate into NiO NPs (see Materials and Methods section) is responsible for quenching the nanocarrier surface basicity by converting exposed N-basic sites (*i.e*. pyridines) into the corresponding N-oxides. Anyway, the subsequent hydrogenation step for the NiO reduction to Ni(0) is thought to take place on the oxidized nanocarrier as well, thus restoring its pristine surface basic character. As a proof of concept, a sample of calcinated N-CNT (N-$CNT_{calc.}$) has been titrated before and after hydrogenation at 360 °C (see Materials and Methods section for details). As Table 1 shows, the calcinated sample does not present any appreciable basic character (entry 1); on the contrary, its basicity grows up after prolonged hydrogenation treatments (entries 2-3). It should be noticed that 24 h hydrogenation do not alter significantly either composition or surface basicity compared to the sample obtained after short time (2 h) hydrogenation (entry 2 *vs*. 3).

Table 1. N-CNT surface basicity determined by acid-base titration and samples composition determined by XPS analyses.

Entry	Sample	Surface basic sites (mmol/g) [a]	Hydrogen. time (h) [b]	Elemental composition [c]			N 1*s* XPS analysis [d]				
				C (%)	N (%)	O (%)	405.4 eV N-oxides	403 eV Py-N-oxide	401.5 eV N-Quaternary	400.5 eV Pyrrole / amines	399 eV Pyridine
1	N-$CNT_{calc.}$	0.04	-	90.5	2.8	6.8	37.4	8.4	21.3	17.7	15.2
2	N-CNT_{H2}	2.44	2	91.4	2.4	6.2	37.0	5.2	21.8	18.8	17.3
3	N-CNT_{H2}	2.77	24	91.5	2.5	5.9	36.9	5.0	18.8	18.6	17.7

[*a*] Measured by acid-base titration for each sample as average values over three independent runs. [*b*] Conducted at 360 °C under a constant stream of H_2 at ambient pressure. [*c*] Determined by integration of the respective XPS peaks at the survey spectrum. [*d*] Atomic percentages calculated on the basis of the best peak fitting.

In the attempt to get additional insights on the process, C *1s* and N *1s* high resolution XPS analyses are recorded on all N-CNT samples and semi quantitative atomic percentages are calculated for each element by fitting the spectra with mixed Gaussian−Lorentzian peaks (Table 1 and Figures S2). Due to the high aspect-ratio of N-CNT samples, XPS analysis reflects the bulk material composition instead of its surface one. Therefore, surface hydrogenation will translate into an only moderate alteration of the XPS profiles. Anyway, the peak fitting of N *1s* core region accounts for an appreciable reduction of the component at 403.0 eV ascribed to pyridine N-oxides together with an equally significant increase of free pyridine nuclei as shown by the increased component at 399.0 eV. This trend well matches with the reduction of oxygen containing functionalities on the composites after hydrogenation. Accordingly, it can be inferred that a thermally induced hydrogenation converts surface pyridine N-oxide into its N-oxide-free counterparts thus justifying the increased material surface basicity. A slight increase of the component around 400 eV can also be thought as a partial surface hydrogenation of N-containing frameworks with the generation of aliphatic amine. This could be responsible for an additional increase of the material surface basicity but any conclusion on that direction remains on a speculative ground due to the complex N-composition of the samples in that region that does not allow to trace out any clear-cut conclusion.

Overall, the nanocarrier surface basicity draws a mechanistic scenario for CO_2 methanation tightly related to that described by Fierro-Gonzalez *et al*.[81] with their ZrO-supported Ni catalyst. Indeed, the inherent basic character of N-CNT acts as a sponge for CO_2 capture thus fostering the generation of local gradients of gas concentration that translate in a higher process efficiency (high X_{CO2} values). Other organic and inorganic basic supports have recently been adopted with the same purpose and in combination with different metal nanoparticles as to join the metal action of H_2 activation/dissociation with an improved CO_2 capture ability from the support.[40, 44-45]

3.4 Study of Ni/N-CNT catalyst stability on stream. The excellent CO_2 methanation performance of Ni/N-CNT is also attributed to the existing interaction between Ni-NPs (metal active phase) and surface N-dopants. Such an interaction controls the dispersion of metal nanoparticles at the N-CNT surface while ensures a tighter interaction of Ni-sites at the nanocarrier. As a matter of fact, selected deactivation phenomena such as NPs leaching or sintering are largely controlled and mitigated throughout the reaction course (*vide infra*).

TEM analysis of the exhaust catalyst (Figure 4A-B) reveals a moderate passivation of the metal active sites caused by the generation of amorphous carbonaceous deposits (coke). TEM at higher magnifications (Figure 4B) show a partial covering of Ni-NPs by carbonaceous layers (white arrows) prevalently formed on the NP side more directly exposed to the stream. Anyway, a large part of NPs surface area remains carbon-free and thus available for the process to occur.

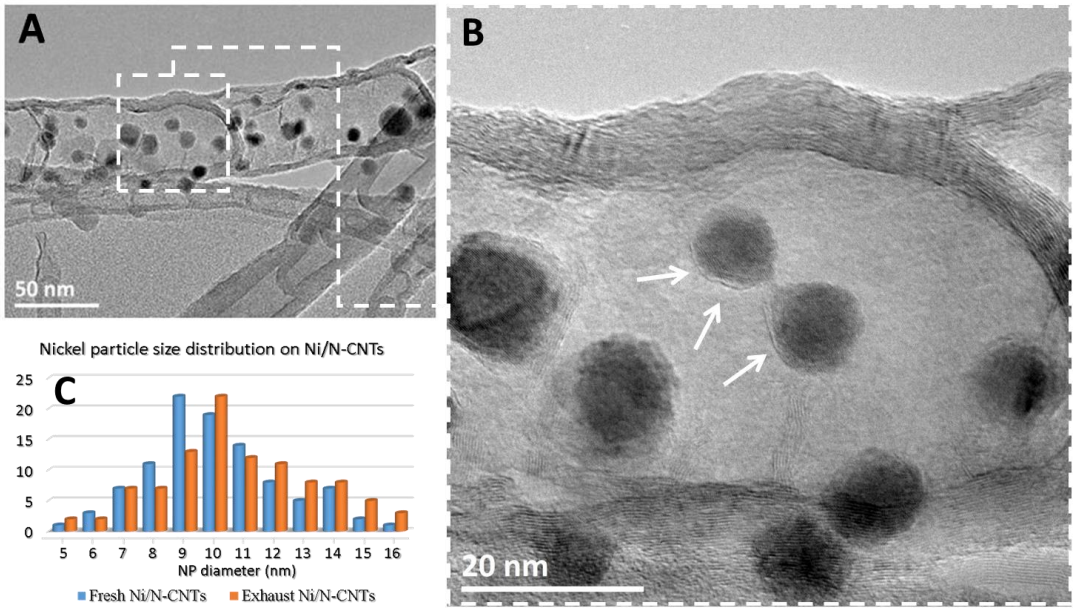

Figure 4. A and **B**: Representative TEM micrographs of the spent Ni/N-CNT catalyst at different magnifications. White arrows on B show the local formation of carbonaceous deposits. **C**: Nickel particle size distribution in freshly prepared Ni/N-CNT (blue histograms) and after long-term catalytic evaluation (orange histograms).

An estimation of coke deposits on the catalyst after 70 h of reaction at a GHSV of 60,000 mL g^{-1} h^{-1} is given by TGA analysis. As Figure S3 shows, the thermogravimetric profile of the

spent catalyst presents a minor shoulder around 390 °C, roughly quantified in about 1.5 wt.% and tentatively ascribed to the formation of low-temperature coke deposits. No evidences for the generation of high- or medium temperature cokes are given for this sample after catalysis.

Although coke formation is among the main causes responsible for nickel-based catalysts deactivation in CO_2 methanation, several reasons can be invoked to explain the markedly high stability of Ni/N-CNT under the operative conditions. Firstly, the high thermal conductivity of the CNT support is supposed to deeply control the formation of local temperature "hot spots" or gradients of temperature inside the catalyst bed thus limiting the occurrence of side-processes responsible for the formation of solid C-deposits around NPs. Secondly, small sized metal particles deactivate for coke passivation less rapidly than larger ones; Stangeland et al. have observed how the higher the Ni particle size the faster the deactivation rate caused by coke deposits.[58] Lastly, but not less importantly, the basic character of the NP support is thought to play an additional role on the control of the catalyst stability on stream. This is in accord to recent findings from some of us in the area of steam- and oxygen-free alkane dehydrogenation (DDH) promoted by highly basic N-doped and metal-free carbon nanomaterials.[82] DDH catalysts also suffer by coke deactivation phenomena and it has been demonstrated that the higher the material surface basicity the lower the formation of coke deposits. Indeed, it is assumed that basic sites make much faster products and reagents desorption rates from the catalyst surface compared to cracking side reactions rates.[82] This trend is indirectly confirmed by other literature reports on CO_2 methanation using acid supports (*i.e.* Al_2O_3) for the metal active phase and where deactivation by coke deposits takes place much faster than in the presence of basic carriers.[83]

The high thermal control at the catalyst bed is additionally thought to have beneficial effects with respect to NPs sintering phenomena. On this ground, TEM micrographs of the spent catalyst are used to confirm the relatively high stability of the heterogeneous system after

catalysis. Figure 4C refers to Ni-NPs size distribution (calculated over 200 particles) for the freshly prepared (blue histograms) and spent (orange histograms) catalyst, the latter obtained after 70 h on stream at a GHSV of 60,000 mL g^{-1} h^{-1} with a H_2-to-CO_2 v/v ratio of 4. Accordingly, Ni-NPs do not undergo any appreciable sintering throughout the reaction course as any minor NP size deviation falls in the experimental error. Once again, surface basicity of N-CNT is claimed to largely prevent sintering phenomena of Ni-NPs by strengthening metal-support interactions. Thermal conductivity of N-CNT could also play a role in the reduction of hot spot formation in the catalyst bed which prevents metal NPs sintering phenomena.

4. CONCLUSIONS

In summary, Ni-NPs decorated N-doped carbon nanotubes (Ni/N-CNT; 10.7 wt.% in Ni) have been synthesized by wet-impregnation/reduction method to give a robust catalyst for CO_2 methanation with specific rates close to 5 $mol_{CH_4} \cdot g_{Ni}^{-1} \cdot h^{-1}$ (GHSV = 120 K mL g^{-1} h^{-1} and H_2-to-CO_2 v/v ratio = 6) that rank among the highest values reported so far in the literature for Ni-based systems. Such performance is ascribed to unique catalyst features that includes: a) short reagents diffusion paths due to the nanoscopic dimensions of N-CNT carrier and the localization of the catalyst active phase (Ni-NPs) at its outer surface only and b) a high thermal conductivity of the support which limits the generation of local "hot spots" during the reaction course. These aspects are of particular relevance for systems operating under dynamic conditions, *i.e.* where H_2-to-CO_2 v/v ratio and GHSVs can change as a function of RE H_2 generation and supply. These fluctuations can be responsible for the generation of temperature gradients and variable steam concentrations at the catalytic bed, potentially causing a decrease of methanation selectivity. In the case of Ni/N-CNT we have demonstrated that at higher GHSV (120 K mL g^{-1} h^{-1} – the highest value tested in the literature so far), an increase of H_2-to-CO_2

v/v ratio from 4 to 6, increases X_{CO2} and S_{CH4} from 75 to 92 % and from 94 to 98 %, respectively. Moreover, the N-doping in N-CNT along with its inherent basic character are thought to play largely beneficial effects in the methanation reaction both in terms of catalyst performance and its stability as a function of time-on-stream. Indeed, N-doping provides preferential binding sites for Ni-NPs growth and stabilization while it contributes to generate CO_2 concentration gradients in proximity of the catalyst active phase. Besides improving the catalyst efficiency, the basic character of the support is also claimed to control the catalyst stability on stream by preventing or reducing its active phase passivation by coke deposits. Indeed, it is assumed that basic sites make much faster products and reagents desorption rates from the catalyst surface compared to cracking side reactions rates. As a matter of fact, dedicated long-term evaluation trials, including tests at variable GHSV and H_2-to-CO_2 ratio, have been used to demonstrate the excellent catalyst stability as a function of time-on-stream. Main deactivation phenomena (*i.e.* NPs leaching or sintering) as well as the active phase passivation by coke deposits seem to hold only negligible effects on the catalyst performance even when methanation is performed under more severe and dynamic conditions.

Overall, Ni/N-CNT lists a series of key features whose combination give rise to an ideal catalytic system for a process at the heart of the chemical energy storage in the renewable energy technology. As a step forward in the field, N-CNTs can be directly grow at the surface of macroscopic and thermal conductive host matrices, *i.e.* carbon felt (CF) or silicon carbide (SiC),[84-85] thus preventing pressure drop phenomena and facilitating the catalyst handling and transportation. Studies in such a direction are currently ongoing in the lab and they will be reported soon elsewhere.

▪ ASSOCIATED CONTENTS

Supporting Information.

The Supporting Information is available free of charge on the ACS Publications website at DOI: …….

Specific rates ($mol_{CH_4}.g_{Ni}^{-1}.h^{-1}$) of various catalytic systems at comparison; Arrhenius plot for Ni/N-CNT in CO_2 methanation; High resolution C *1s* and N *1s* XPS spectra for calcinated and hydrogenated N-CNT samples; TGA/DTG profiles Ni/N-CNT sample after 70 h run in CO_2 methanation (PDF)

▪ AUTHOR INFORMATION

Corresponding Authors

* Cuong Duong-Viet; E-mail: *duongvietcuong@humg.edu.vn*.

* Cuong Pham-Huu; E-mail: *cuong.pham-huu@unistra.fr*

* Giuliano Giambastiani; E-mail: *giambastiani@unistra.fr*

ORCID Giuliano Giambastiani: 0000-0002-0315-3286

Notes

The authors declare no competing financial interest.

▪ ACKNOWLEDGEMENTS

G. G. and C. P.-H. thank the TRAINER project (Catalysts for Transition to Renewable Energy Future) of the "Make our Planet Great Again" program (Ref. ANR-17-MPGA-0017) for support. The Italian team would also like to thank the Italian MIUR through the PRIN 2015 Project SMARTNESS (2015K7FZLH) "Solar driven chemistry: new materials for photo- and electrocatalysis" for financial support to this work. W. W. would like to thank the China Scholarship Council (CSC) for financial support during his Ph.D. stay at the ICPEES. SEM analysis was carried out at the joint SEM platform of the ICPEES-IPCMS and T. Romero (ICPEES) is gratefully acknowledged for performing experiments.

REFERENCES

1. G. Centi; Perathoner, S., Opportunities and Prospects in the Chemical Recycling of Carbon Dioxide to Fuels. *Catal. Today* **2009**, *148*, 191-205.
2. European Commission - A Roadmap for moving to a competitive low carbon economy in 2050, **2011**.
3. W. Li; H. Wang; X. Jiang; J. Zhu; Z. Liu; X. Guo; Song, C., A Short Review of Recent Advances in CO_2 Hydrogenation to Hydrocarbons over Heterogeneous Catalysts. *RSC Adv.* **2018**, *8*, 7651-7669.
4. J. Ma; N. Sun; X. Zhang; N. Zhao; F. Xiao; W. Wei; Sun, Y., A Short Review of Catalysis for CO_2 Conversion. *Catal. Today* **2009**, *148*, 221-231.
5. P. G. Jessop; F. Joo; Tai, C. C., Recent Advances in the Homogeneous Hydrogenation of Carbon Dioxide. *Coord. Chem. Rev.* **2004**, *248*, 2425-2442.
6. W. Wang; S. Wang; X. Ma; Gong, J., Recent Advances in Catalytic Hydrogenation of Carbon Dioxide. *Chem. Soc. Rev.* **2011**, *40*, 3703-3727.
7. S. Saeidi; N. A. S. Amin; Rahimpour, M. R., Hydrogenation of CO_2 to Value-Added Products - A Review and Potential Future Developments. *J. CO_2 Util.* **2014**, *5*, 66-81.
8. G. Centi; Perathoner, S., CO_2-Based Energy Vectors for the Storage of Solar Energy. *Greenhouse Gases: Sci. Technol.* **2011**, *1*, 21-35.

9. L. Zhou; Q. Wang; L. Ma; J. Chen; J. Ma; Zi, Z., CeO_2 Promoted Mesoporous Ni/γ-Al_2O_3 Catalyst and its Reaction Conditions for CO_2 Methanation. *Catal. Lett.* **2015**, *145*, 612-619.
10. A. Westermann; B. Azambre; M. C. Bacariza; I. Graca; M. F. Ribeiro; J. M. Lopes; Henriques, C., Insight into CO_2 Methanation Mechanism over NiUSY Zeolites: An Operando IR Study. *Appl. Catal. B* **2015**, *174*, 120-125.
11. D. C. Upham; A. R. Derk; S. Sharma; H. Metiu; McFarland, E. W., CO_2 Methanation by Ru-Doped Ceria: the Role of the Oxidation State of the Surface. *Catal. Sci. Technol.* **2015**, *5*, 1783-1791.
12. N. Shimoda; D. Shoji; K. Tani; M. Fujiwara; K. Urasaki; R. Kikuchi; Satokawa, S., Role of Trace Chlorine in Ni/TiO_2 Catalyst for CO Selective Methanation in Reformate Gas. *Appl. Catal. B* **2015**, *174*, 486-495.
13. R. Razzaq; C. Li; M. Usman; K. Suzuki; Zhang, S., A Highly Active and Stable Co_4N/γ-Al_2O_3 Catalyst for CO and CO_2 Methanation to Produce Synthetic Natural Gas (SNG). *Chem. Eng. J.* **2015**, *262*, 1090-1098.
14. S. K. Beaumont; S. Alayoglu; C. Specht; W. D. Michalak; V. V. Pushkarev; J. Guo; N. Kruse; Somorjai, G. A., Combining in Situ NEXAFS Spectroscopy and CO_2 Methanation Kinetics To Study Pt and Co Nanoparticle Catalysts Reveals Key Insights into the Role of Platinum in Promoted Cobalt Catalysis. *J. Am. Chem. Soc.* **2014**, *136*, 9898-9901.
15. F. Wang; C. Li; X. Zhang; M. Wei; D. G. Evans; Duan, X., Catalytic Behavior of Supported Ru Nanoparticles on the {1 0 0}, {1 1 0}, and {1 1 1} Facet of CeO_2. *J. Catal.* **2015**, *329*, 177-186.
16. M. D. Porosoff; B. Yan; Chen, J. G., Catalytic Reduction of CO_2 by H_2 for Synthesis of CO, Methanol and Hydrocarbons: Challenges and Opportunities. *Energy Environ. Sci.* **2016**, *9*, 62-73.
17. C. G. Visconti; M. Martinelli; L. Falbo; A. Infantes-Molina; L. Lietti; P. Forzatti; G. Iaquaniello; E. Palo; B. Picutti; Brignoli, F., CO_2 Hydrogenation to Lower Olefins on a High Surface Area K-Promoted Bulk Fe-Catalyst. *Appl. Catal. B* **2017**, *200*, 530-542.
18. P. Gao; S. Li; X. Bu; S. Dang; Z. Liu; H. Wang; L. Zhong; M. Qiu; C. Yang; J. Cai; W. Wei; Sun, Y., Direct Conversion of CO_2 into Liquid Fuels with High Selectivity over a Bifunctional Catalyst. *Nat. Chem.* **2017**, *9*, 1019-1024.
19. H. Song; N. Zhang; C. Zhong; Z. Liu; M. Xiao; Gai, H., Hydrogenation of CO_2 into Formic Acid Using a Palladium Catalyst on Chitin. *New J. Chem.* **2017**, *41*, 9170-9177.

20. K. Larmier; W. C. Liao; S. Tada; E. Lam; R. Verel; A. Bansode; A. Urakawa; A. Comas-Vives; Coperet, C., CO_2-to-Methanol Hydrogenation on Zirconia-Supported Copper Nanoparticles: Reaction Intermediates and the Role of the Metal–Support Interface. *Angew. Chem. Int. Ed.* **2017**, *56*, 2318-2323.
21. X. Jiang; N. Koizumi; X. Guo; Song, C.; , A. C., B,; 2015, -., 173-185, Bimetallic Pd–Cu Catalysts for Selective CO_2 Hydrogenation to Methanol. *Appl. Catal. B* **2015**, *170-171*, 173-185.
22. S. Bai; Q. Shao; P. Wang; Q. Dai; X. Wang; Huang, X., Highly Active and Selective Hydrogenation of CO_2 to Ethanol by Ordered Pd–Cu Nanoparticles. *J. Am. Chem. Soc.* **2017**, *139*, 6827-6830.
23. www.powertogas.info/power-to-gas/pilotprojekte-im-ueberblick/audi-e-gas-projekt/
24. M. Jentsch; T. Trost; Sterner, M., Optimal Use of Power-to-Gas Energy Storage Systems in an 85% Renewable Energy Scenario. *Energy Procedia* **2014**, *46*, 254-261.
25. K. Hashimoto; N. Kumagai; K. Izumiya; H. Takano; Kato, Z., The Production of Renewable Energy in the Form of Methane Using Electrolytic Hydrogen Generation. *Energy Sustain. Soc.* **2014**, *4*, 17.
26. F. D.Meylan; V. Moreau; Erkman, S., Material Constraints Related to Storage of Future European Renewable Electricity Surpluses with CO_2 Methanation. *Energy Policy* **2016**, *94*, 366-376.
27. S. Kattel; P. Liu; Chen, J. G., Tuning Selectivity of CO_2 Hydrogenation Reactions at the Metal/Oxide Interface. *J. Am. Chem. Soc.* **2017**, *139*, 9739-9754.
28. J. Martins; N. Batail; S. Silva; S. Rafik-Clement; A. Karelovic; D.P. Debecker; A. Chaumonnot; Uzio, D., CO_2 Hydrogenationwith Shape-Controlled Pd Nanoparticles Embedded in Mesoporous Silica: Elucidating Stability and Selectivity Issues. *Catal. Commun.* **2015**, *58*, 11-15.
29. J. Zheng; C. Wang; W. Chu; Y. Zhou; Köhler, K., CO_2 Methanation over Supported Ru/Al_2O_3 Catalysts: Mechanistic Studies by In situ Infrared Spectroscopy. *ChemistrySelect* **2016**, *1*, 3197-3203.
30. S. Abate; C. Mebrahtu; E. Giglio; F. Deorsola; S. Bensaid; S. Perathoner; R. Pirone; Centi, G., Catalytic Performance of γ-Al_2O_3–ZrO_2–TiO_2–CeO_2 Composite Oxide Supported Ni-Based Catalysts for CO_2 Methanation. *Ind. Eng. Chem. Res.* **2016**, *55*, 4451-4460.
31. N. Bette; J. Thielemann; M. Schreiner; Mertens, F., Methanation of CO_2 over a (Mg,Al)Ox Supported Nickel Catalyst Derived from a (Ni,Mg,Al)-Hydrotalcite-like Precursor. *ChemCatChem* **2016**, *8*, 2903-2906.

32. H. Zhang; Y. Dong; W. Fang; Lian, Y., Effects of Composite Oxide Supports on Catalytic Performance of Ni-Based Catalysts for CO Methanation. *Chin. J. Catal.* **2013**, *34*, 330-335.
33. I. Kiendl; M. Klemm; A. Clemens; Herrman, A., Dilute Gas Methanation of Synthesis Gas from Biomass Gasification. *Fuel* **2014**, *123*, 211-217.
34. M.C. Seemann; T.J. Schildhauer; Biollaz, S. M. A., Fluidized Bed Methanation of Wood-Derived Producer Gas for the Production of Synthetic Natural Gas. *Ind. Eng. Chem. Res.* **2010**, *49*, 7034-7038.
35. S. Danaci; L. Protasova; J. Lefevere; L. Bedel; R. Guilet; Marty, P., Efficient CO_2 Methanation over Ni/Al_2O_3 Coated Structured Catalysts. *Catal. Today* **2016**, *273*, 234-243.
36. C. Janke; M.S. Duyar; M. Hoskins; Farrauto, R., Catalytic and Adsorption Studies for the Hydrogenationof CO_2 to Methane. *Appl. Catal. B-Environ.* **2014**, *152-153*, 184-191.
37. D. Schlereth; P. J. Donaubauer; Hinrichsen, O., Metallic Honeycombs as Catalyst Supports for Methanation of Carbon Dioxide. *Chem. Eng. Technol.* **2015**, *38*, 1845-1852.
38. W. Wang; W. Chu; N. Wang; W. Yang; Jiang, C., Mesoporous Nickel Catalyst Supported on Multi-Walled Carbon Nanotubes for Carbon Dioxide Methanation. *Int. J. Hydrogen Energy* **2016**, *41*, 967-975.
39. L. Li; J. Zheng; Y. Liu; W. Wang; Q. Huang; Chu, W., Impacts of SiC Carrier and Nickel Precursor of NiLa/support Catalysts for CO_2 Selective Hydrogenation to Synthetic Natural Gas (SNG). *ChemistrySelect* **2017**, *2*, 3750-3757.
40. L. Roldán; Y. Marco; García-Bordejé, E., Origin of the Excellent Performance of Ru on Nitrogen-Doped Carbon Nanofibers for CO_2 Hydrogenation to CH_4. *ChemSusChem* **2017**, *10*, 1139-1144.
41. M. Frey; A. Bengaouer; G. Geffraye; D. Edouard; Roger, A.-C., Aluminum Open Cell Foams as Efficient Supports for Carbon Dioxide Methanation Catalysts: Pilot-Scale Reaction Results. *Energy Technol.* **2017**, *5*, 2078-2085.
42. M. Frey; T. Romero; A.-C. Rogera; Edouard, D., Open Cell foam Catalysts for CO_2 Methanation: Presentation of Coating Procedures and *in situ* Exothermicity Reaction Study by Infrared Thermography. *Catal. Today* **2016**, *273*, 83-90.
43. J. Amadou; K. Chizari; M. Houlle´; I. Janowska; O. Ersen; D. Bégin; Pham-Huu, C., N-Doped Carbon Nanotubes for Liquid-Phase C=C Bond Hydrogenation. *Catal. Today* **2008**, *138*, 62-68.
44. G.-P. Hao; W.-C. Li; D. Qian; Lu, A.-H., Rapid Synthesis of Nitrogen-Doped Porous Carbon Monolith for CO_2 Capture. *Adv. Mater.* **2010**, *22*, 853-857.

45. P. A. Ussa Aldana; F. Ocampo; K. Kobl; B. Louis; F. Thibault-Starzyk; M. Daturi; P. Bazin; S. Thomas; Roger, A. C., Catalytic CO_2 Valorization into CH_4 on Ni-Based Ceria-Zirconia. Reaction Mechanism by Operando IR Spectroscopy. *Catal. Today* **2013**, *215*, 201-207.
46. N. Hollingsworth; S. F. R. Taylor; M. T. Galante; J. Jacquemin; C. Longo; K. B. Holt; N. H. de Leeuw; Hardacre, C., Reduction of Carbon Dioxide to Formate at Low Overpotential Using a Superbase Ionic Liquid. *Angew. Chem. Int. Ed.* **2015**, *54*, 14164-14168.
47. G. Tuci; J. Filippi; H. Ba; A. Rossin; L. Luconi; C. Pham-Huu; F. Vizza; Giambastiani, G., How to Teach an Old Dog New (Electrochemical) Tricks: Aziridine-Functionalized CNTs as Efficient Electrocatalysts for the Selective CO_2 Reduction to CO. *J. Mater. Chem. A* **2018**, *6*, 16382-16389.
48. J.-N. Park; McFarland, E. W., A highly Dispersed Pd–Mg/SiO_2 Catalyst Active for Methanation of CO_2. *J. Catal.* **2009**, *266*, 92-97.
49. Z.-W. Zhao; X. Zhou; Y.-N. Liu; C.-C. Shen; C.-Z. Yuan; Y.-F. Jiang; S.-J. Zhao; L.-B. Ma; T.-Y. Cheang; Xu, A.-W., Ultrasmall Ni Nanoparticles Embedded in Zr-Based MOFs Provide High Selectivity for CO_2 Hydrogenation to Methane at Low Temperatures. *Catal. Sci. Technol.* **2018**, *8*, 3160-3165.
50. Y. Wang; H. Arandiyan; J. Scott; H. Dai; Amal, R., Hierarchically Porous Network-Like Ni/Co3O4: Noble Metal-Free Catalysts for Carbon Dioxide Methanation. *Adv. Sustainable Syst.* **2018**, *2*, 1700119.
51. Y. Tang; Y. Kobayashi; C. Tassel; T. Yamamoto; Kageyama, H., Hydride-Enhanced CO_2 Methanation: Water-Stable $BaTiO_2.4H_{0.6}$ as a New Support. *Adv. Energy Mater.* **2018**, 1800800.
52. W. Zhen; B. Li; G. Lu; Ma, J., Enhancing Catalytic Activity and Stability for CO_2 Methanation on Ni@MOF-5 via Control of Active Species Dispersion. *Chem. Commun.* **2015**, *51*, 1728-1731.
53. W. Gac; W. Zawadzki; G. Słowik; A. Sienkiewicz; Kierys, A., Nickel Catalysts Supported on Silica Microspheres for CO_2 Methanation. *Micropor. Mesopor. Mat.* **2018**, *272*, 79-91.
54. Q. Liu; S. Wang; G. Zhao; H. Yang; M. Yuan; X. An; H. Zhou; Y. Qiao; Tian, Y., CO_2 Methanation over Ordered Mesoporous NiRu-Doped CaO-Al_2O_3 Nanocomposites with Enhanced Catalytic Performance. *Int. J. Hydrogen Energy* **2018**, *43*, 239-250.
55. M.C. Bacariza; I. Graça; S.S. Bebiano; J.M. Lopes; Henriques, C., Micro- and Mesoporous Supports for CO_2 Methanation Catalysts: A Comparison Between SBA-15, MCM-41 and USY Zeolite. *Chem. Eng. Sci.* **2018**, *175*, 72-83.

56. M. Romero-Sáez; A. B. Dongil; N. Benito; R. Espinoza-González; N. Escalona; Gracia, F., CO_2 Methanation over Nickel-ZrO_2 Catalyst Supported on Carbon Nanotubes: A Comparison Between two Impregnation Strategies. *Appl. Catal. B-Environ.* **2018**, *237*, 817-825.
57. M. Guo; Lu, G., The effect of Impregnation Strategy on Structural Characters and CO_2 Methanation Properties over MgO Modified Ni/SiO_2 Catalysts. *Catal. Commun.* **2014**, *54*, 55-60.
58. K. Stangeland; D. Y. Kalai; H. Li; Yu, Z., Active and Stable Ni Based Catalysts and Processes for Biogas Upgrading: The Effect of Temperature and Initial Methane Concentration on CO_2 Methanation. *Appl. Energy* **2018**, *227*, 206-212.
59. J. Liu; C. Li; F. Wang; S. He; H. Chen; Y. Zhao; M. Wei; D. G. Evans; Duan, X., Enhanced Low-Temperature Activity of CO_2 Methanation over Highly-Dispersed Ni/TiO_2 Catalyst. *Catal. Sci. Technol.* **2013**, *3*, 2627-2633.
60. J. K. Kesavan; I. Luisetto; S. Tuti; C. Meneghini; G. Iucci; C. Battocchio; S. Mobilio; S. Casciardi; Sisto, R., Nickel Supported on YSZ: The Effect of Ni Particle Size on the Catalytic Activity for CO_2 Methanation. *J. CO_2 Util.* **2018**, *23*, 200-211.
61. J. K. Kesavan; I. Luisetto; S. Tuti; C. Meneghini; C. Battocchio; Iucci, G., Ni Supported on YSZ: XAS and XPS Characterization and Catalytic Activity for CO_2 Methanation. *J. Mater. Sci.* **2017**, *52*, 10331-10340.
62. J. Ashok; M.L. Ang; Kawi, S., Enhanced Activity of CO_2 Methanation over Ni/CeO_2-ZrO_2 Catalysts: Influence of Preparation Methods. *Catal. Today* **2017**, *281*, 304-311.
63. I. Graca; L. V. González; M. C. Bacariza; A. Fernandes; C. Henriques; J. M. Lopes; Ribeiro, M. F., CO2 Hydrogenation into CH_4 on NiHNaUSY Zeolites. *Appl. Catal. B-Environ.* **2014**, *147*, 101-110.
64. G. Zhou; H. Liu; K. Cui; H. Xie; Z. Jiao; G. Zhang; K. Xiong; Zheng, X., Methanation of Carbon Dioxide over Ni/CeO_2 Catalysts: Effects of Support CeO_2 Structure. *Int. J. Hydrogen Energy* **2017**, *42*, 16108-16117.
65. G. Zhou; H. Liu; K. Cui; A. Jia; G. Hu; Z. Jiao; Y. Liu; Zhang, X., Role of Surface Ni and Ce Species of Ni/CeO_2 Catalyst in CO_2 Methanation. *Appl. Surf. Sci.* **2016**, *383*, 248-252.
66. B. Mutz; M. Belimov; W. Wang; P. Sprenger; M.-A. Serrer; D. Wang; P. Pfeifer; W. Kleist; Grunwaldt, J.-D., Potential of an Alumina-Supported Ni_3Fe Catalyst in the Methanation of CO_2: Impact of Alloy Formation on Activity and Stability. *ACS Catal.* **2017**, *7*, 6802-6814.

67. A. Vita; C. Italiano; L. Pino; P. Frontera; M. Ferraro; Antonucci, V., Activity and Stability of Powder and Monolith-Coated Ni/GDC Catalysts for CO_2 Methanation. *Appl. Catal. B-Environ.* **2018**, *226*, 384-395.
68. C. Duong-Viet; L. Truong-Phuoc; T. Tran-Thanh; J.-M. Nhut; L. Nguyen-Dinh; I. Janowska; D. Begin; Pham-Huu, C., Nitrogen-Doped Carbon Nanotubes Decorated Silicon Carbide as a Metal-Free Catalyst for Partial Oxidation of H_2S. *Appl. Catal. A-Gen.* **2014**, *482*, 397-406.
69. K. Chizari; I. Janowska; M. Houllé; I. Florea; O. Ersen; T. Romero; P. Bernhardt; M. J. Ledoux; Pham-Huu, C., Tuning of Nitrogen-Doped Carbon Nanotubes as Catalyst Support for Liquid-Phase Reaction. *Appl. Catal. A-Gen.* **2010**, *380*, 72-80.
70. P. Azadi; R. Farnood; Meier, E., Preparation of Multiwalled Carbon Nanotube-Supported Nickel Catalysts Using Incipient Wetness Method. *J. Phys. Chem. A* **2010**, *114*, 3962-3968.
71. O. Ersen; C. Hirlimann; M. Drillon; J. Werckmann; F. Tihay; C. Pham-Huu; C. Crucifix; Schultz, P., 3D-TEM Characterization of Nanometric Objects. *Solid State Sci.* **2007**, *9*, 1088-1098.
72. O. Ersen; I. Florea; C. Hirlimann; Pham-Huu, C., Exploring Nanomaterials with 3D Electron Microscopy. *Mater. Today* **2015**, *18*, 395-408.
73. A. Ameli; M. Arjmand; P. Pötschke; B. Krause; Sundararaj, U., Effects of Synthesis Catalyst and Temperature on Broadband Dielectric Properties of Nitrogen-Doped Carbon Nanotube/Polyvinylidene Fluoride Nanocomposites. *Carbon* **2016**, *106*, 260-278.
74. Y. Zhong; M. Jaidann; Y. Zhang; G. Zhang; H. Liu; M. I. Ionescu; R. Li; X. Sun; H. Abou-Rachid; Lussier, L.-S., Synthesis of High Nitrogen Doping of Carbon Nanotubes and Modeling the Stabilization of Filled DAATO@CNTs (10,10) for Nanoenergetic Materials. *J. Phys. Chem. Solids* **2010**, *71*, 134-139.
75. I. Florea; O. Ersen; R. Arenal; D. Ihiawakrim; C. Messaoudi; K. Chizari; I. Janowska; Pham-Huu, C., 3D Analysis of the Morphology and Spatial Distribution of Nitrogen in Nitrogen-Doped Carbon Nanotubes by Energy-Filtered Transmission Electron Microscopy Tomography. *J. Am. Chem. Soc.* **2012**, *134*, 9672-9680.
76. J. Gao; Y. Wang; Y. Ping; D. Hu; G. Xu; F. Gu; Su, F., A Thermodynamic Analysis of Methanation Reactions of Carbon Oxides for the Production of Synthetic Natural Gas. *RSC Adv.* **2012**, *2*, 2358-2368.
77. F. Koschany; D. Schlereth; Hinrichsen, O., On the Kinetics of the Methanation of Carbon Dioxide on Coprecipitated $NiAl(O)_x$. *Appl. Catal. B* **2016**, *181*, 504-516.

78. A. Yamaguchi; Iglesia, E., Catalytic Activation and Reforming of Methane on Supported Palladium Clusters. *J. Catal.* **2010**, *274*, 52-63.
79. D. Mei; J. Hun Kwak; J. Hu; S. June Cho; J. Szanyi; L. F. Allard; Peden, C. H. F., Unique Role of Anchoring Penta-Coordinated Al^{3+} Sites in the Sintering of γ-Al_2O_3-Supported Pt Catalysts. *J. Phys. Chem. lett.* **2010**, *1*, 2688-2691.
80. D. Tasis; N. Tagmatarchis; A. Bianco; Prato, M., Chemistry of Carbon Nanotubes. *Chem. Rev.* **2006**, *106*, 1105-1136.
81. A. Solis-Garcia; J. F. Louvier-Hernandez; A. Almendarez-Camarillo; Fierro-Gonzalez, J. C., Participation of Surface Bicarbonate, Formate and Methoxy Species in the Carbon Dioxide Methanation Catalyzed by ZrO_2-Supported Ni. *Appl. Catal. B-Environ.* **2017**, *218*, 611-620.
82. G. Tuci; M. Pilaski; H. Ba; A. Rossin; L. Luconi; S. Caporali; C. Pham-Huu; R. Palkovits; Giambastiani, G., Unraveling Surface Basicity and Bulk Morphology Relationship on Covalent Triazine Frameworks with Unique Catalytic and Gas Adsorption Properties. *Adv. Funct. Mater.* **2017**, *27*, 1605672.
83. D. Pakhare; Spivey, J., A Review of Dry (CO_2) Reforming of Methane over Noble Metal Catalysts. *Chem. Soc. Rev.* **2014**, *43*, 7813-7837.
84. K. Chizari; A. Deneuve; O. Ersen; I. Florea; Y. Liu; D. Edouard; I. Janowska; D. Begin; Pham-Huu, C., Nitrogen-Doped Carbon Nanotubes as a Highly Active Metal-Free Catalyst for Selective Oxidation. *ChemSusChem* **2012**, *5*, 102-108.
85. H. Ba; Y. Liu; C. Duong-Viet; L. Truong-Phuoc; Z. El Berichi; J. M. Nhut; M. J. Ledoux; Pham-Huu, C., Silicon Carbide Foam as a Porous Support Platform for Catalytic Applications. *New J. Chem.* **2016**, *40*, 4285-4299.

TOC graphic